applied sciences

MDPI

Article

Combined Prediction Method for Thermal Conductivity of Asphalt Concrete Based on Meso-Structure and Renormalization Technology

Jiaqi Chen [1], Xingzao Chen [1], Hancheng Dan [1,*] and Lanchun Zhang [2]

[1] Department of Civil Engineering, Central South University, Changsha 410075, China; chenjiaqi@csu.edu.cn (J.C.); chenxingzao@csu.edu.cn (X.C.)
[2] Friendship International Engineering Consulting Co., Ltd., Changsha 410005, China; zlc904069@163.com
* Correspondence: danhancheng@csu.edu.cn; Tel.: +86-13874934466

Abstract: Pavement temperature field affects pavement service life and the thermal environment the near road surface; thus, is important for sustainable pavement design. This paper developed a combined prediction method for the thermal conductivity of asphalt concrete based on meso-structure and renormalization technology, which is critical for determining the pavement temperature field. The accuracy of the combined prediction method was verified by laboratory experiments. Using the tested and proven model, the effect of coarse aggregate type, shape, content, spatial orientation, air void of asphalt concrete, and steel fiber on the effective thermal conductivity was analyzed. The analysis results show that the orientation angle and aspect ratio of the aggregate have a combined effect on thermal conductivity. In general, when the aggregate orientation is parallel with the heat conduction direction, the effective thermal conductivity of asphalt concrete in that direction tends to be greater. The effective thermal conductivity of asphalt concrete decreases with the decrease of coarse aggregate content or steel fiber content or with the increase of porosity, and it increases with the increase of the effective thermal conductivity of coarse aggregate.

Keywords: meso-structure; asphalt concrete; effective thermal conductivity; random aggregate technique; discrete element; renormalization

Citation: Chen, J.; Chen, X.; Dan, H.; Zhang, L. Combined Prediction Method for Thermal Conductivity of Asphalt Concrete Based on Meso-Structure and Renormalization Technology. *Appl. Sci.* **2022**, *12*, 857. https://doi.org/10.3390/app12020857

Academic Editors: Andrea Dorigato and Doo-Yeol Yoo

Received: 29 November 2021
Accepted: 12 January 2022
Published: 14 January 2022

1. Introduction

A phenomenon in which temperatures in rural areas are lower than in cities has been referred to the urban heat island (UHI) effect [1]. UHI has a direct impact on urban livability, including a decrease in environmental quality, an increase in thermal discomfort, and an increase in heat-related health issues [2]. Satellite images demonstrate that pavements are a substantial source of thermal activity and heat radiation, particularly in urban areas [1]. Ninety percent of solar energy is absorbed by asphalt pavement, as well as warmth that builds within the pavement, increasing its temperature. Studies have shown that hot pavement has a significant impact on the near-surface heat island. The UHI impact is exacerbated as heat from the pavement is released into the atmosphere via convection and effective radiation [3,4]. Thermal conductivity is a critical material of parameters that determine the temperature field of the pavement, and it is essential for evaluating numerous pavement methods for UHI mitigation [5]. Asphalt concrete is a viscoelastic material, and under normal circumstances, the smaller the thermal conductivity, the slower the heat conduction [6]. Pavement mechanical qualities and temperature distribution are substantially affected by the thermal conductivity of asphalt concrete, which also has a knock-on impact on pavement service life and the urban heat island effect [7,8]. Understanding the thermal conductivity of asphalt concrete is critical for estimating the thermodynamic performance of pavement, studying the efficiency of the heat transfer

from road surface to subgrade, alleviating the UHI effect, and promoting the sustainable development of pavement.

Experimentation is now the most used approach for determining the thermal conductivity of asphalt concrete. The slab technique, the guarded heat-flow meter method, the transient plane heat source method, and the hot-wire method are all common methods to measure thermal conductivity in thermal conductivity studies [9–11]. Shi et al. investigated the effects of expanding polypropylene beads and adding graphite powder on the thermal conductivity of HMA [12]. Shatarat et al. examined the thermal conductivity of permeable concrete by replacing it with recycled coarse aggregate and recycled asphalt pavement for natural aggregate [13]. Pan et al. studied the thermal conductivity of conductive asphalt concrete using seven different aggregates and two conductive fillers [14]. Pawel et al. analyzed various aggregates, combinations, and air voids for their impact on thermal conductivity [15]. Although these experimental methods are commonly used and simple to operate, there are still some limitations in the experiment. Expensive measuring devices and a huge number of specimens are required in the experiment, which consume a large amount of measurement time and economic costs.

As a heterogeneous composite material, thermal conductivity, volumetric fractions, and distributions of each component in asphalt concrete all affect the overall effective thermal conductivity of the material. Costs associated with experiments may be considerably reduced by developing an analytical model to forecast effective thermal conductivity based on the heterogeneous meso-structure of asphalt concrete. According to the thermal conductivity and volumetric fractions of every component, analysis models for composite material thermal conductivity have been developed by researchers, such as the parallel model, series model, Maxwell-Eucken model, effective medium theory model, and Bruggeman's equation [16–20]. However, as these models are usually based on specific aggregate distribution forms where the distribution patterns of the two components in asphalt concrete are simple and different from the heterogeneous meso-structure of real asphalt concrete, and the thermal conductivity that is predicted is not the real situation. At present, it is possible to obtain information about the real spatial distribution of aggregate in the asphalt concrete through deep learning image recognition technology and X-ray CT scanning technology to assist modeling [21,22]. With the use of a computer model, the thermal conductivity, dynamic modulus, fracture energy, and creep stiffness of asphalt concrete can be accurately predicted. Some sophisticated heterogeneous meso-structure models have been developed to simulate asphalt concrete [23–27]. When the meso-structure model is established to study the thermal performance of asphalt concrete, the complex aggregate geometry shapes and the volumetric fractions of each component should be considered. To simulate it more realistically, a lot of meshes need to be generated, which leads to the increase of model computation and difficulty in the modeling process. This study proposed renormalization methods for calculating three-dimensional meso-structure thermal conductivity, taking into account the distribution of every component [28]. This approach is dependent on the exact solution of the equivalent thermal conductivity of a set of four cell grids (2×2), and the effective thermal conductivity was calculated layer by layer through using the space-scale upscaling method. However, this method usually needs to extract the two-dimensional cross section image of composite material, which may be inconvenient for batch virtual modeling analysis. Although there are some models that can calculate thermal conductivity, a more efficient one is still needed.

2. Objectives

The principal goal of this research is just to establish a method for calculating the effective thermal conductivity of asphalt concrete using a combination method of three-dimensional meso-structure and the renormalization technique. Considering the complexity of the three-dimensional geometry and the potential relationship between the coarse aggregate two-dimensional picture and the three-dimensional geometry, a single aggregate three-dimensional geometry was randomly generated by using an image-aided

method. The generated three-dimensional aggregates were then loaded with PFC3D, and the three-dimensional meso-structure of asphalt concrete was constructed according to aggregate gradation. The asphalt concrete model was divided into several small volume units with a single thermal conductivity, and the total thermal conductivity of the model was determined utilizing the renormalization technique. Based on the validated DE model, the effects of air void, coarse aggregate shape, spatial orientation, content, type, and steel fiber on the effective thermal conductivity were analyzed.

3. Prediction the Effective Thermal Conductivity of Three-Dimensional Meso-Structures

3.1. Structure Generation

Throughout this research, it was assumed that the asphalt concrete was a composite material consisting of coarse aggregates and a fine aggregate matrix (FAM). The FAM is a blend of asphalt, mineral powder, and fine aggregate with a particle size of less than 2.36 mm. Coarse aggregates are made up of particles larger than 2.36 mm in diameter. A three-dimensional heterogeneous meso-structure model of asphalt concrete has been created using an image-aided technique [29], and the process of generating the three-dimensional model can be summarized as follows.

(1) We developed an aggregate image dataset using Aggregate Image System (AIMS) to capture a batch of two-dimensional projections of aggregates with varying particle sizes. The two-dimensional projections of aggregates were obtained as a binary image by AIMS. Through MATLAB, we extracted a number of control points on the edges of the two-dimensional projection of aggregate, and then connected these control points in turn to obtain the polygon representing the two-dimensional projection contour shape of the aggregate. The experiment setup is depicted in Figure 1, as well as various instances of the polygonal representations of the relevant aggregate pictures.

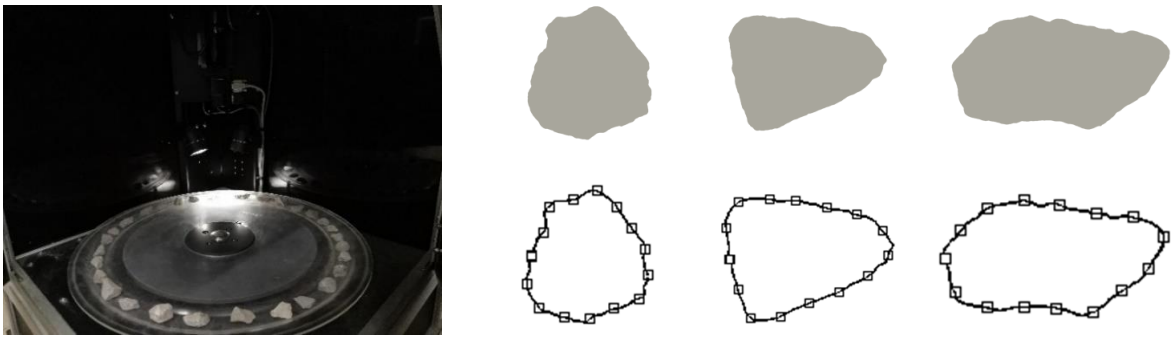

(**a**) (**b**)

Figure 1. (**a**) Experimental setup; (**b**) instances of aggregate pictures and polygons.

(2) We picked at random a two-dimensional aggregate projection (hereafter referred to as P) from the dataset of aggregate images according to the prescribed gradation. A two-dimensional projection had a primary axis that could be determined (P). The longest diagonal line l for every polygon was used to determine its major axis. We placed P on the XOZ major plane; then, we readjusted the position of P so that the midpoint of the main axis coincided with the origin of the XOZ plane, and the main axis fell in the direction of the Z axis, thereby determining the X, Z of all vertices of the two-dimensional projection. Next, we took the origin O as the center and reduced P as a whole by a certain proportion. To create a polygon smaller than P, we linked half of the vertices of the polygon. The vertices on P could not have the same y-coordinates and they were reallocated afterwards.

(3) For the sake of structural of three-dimensional aggregate, Equation (1) was used to estimate a maximum aggregate thickness in the direction of the y-axis.

$$H_{\max} = \alpha L_x \tag{1}$$

where H_{max} is the maximum aggregate thickness; L_x is the maximum width of P parallel to the x-axis; α is a number that is more than zero but less than one. Aggregate surfaces will get flatter as the value of α decreases.

(4) The bottom and top restrictions for the y coordinates of each polygon were determined according to the height of aggregate, and the y coordinates of each vertex were randomly generated within the lower and upper limits. Figure 2 illustrates a schematic diagram of all vertices of the generated three-dimensional aggregate.

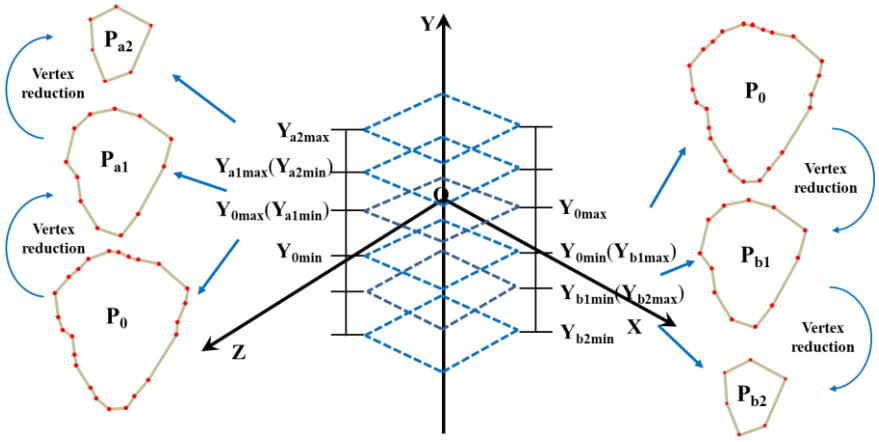

Figure 2. A schematic diagram of the three-dimensional aggregate vertices.

(5) TXT files of all vertex coordinates of the obtained three-dimensional aggregates were converted into three-dimensional model files in STL format through MATLAB. Then the STL files of the aggregates were imported into the PFC3D for modeling. Figure 3 illustrates several instances of 3-D aggregates generated.

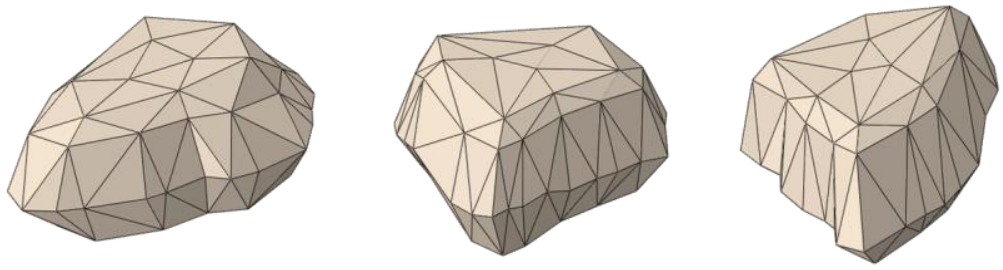

Figure 3. Several instances of generated three-dimensional aggregates.

(6) In the three-dimensional boundary of the heterogeneous model of asphalt concrete, based on a given gradation, small balls were randomly distributed with corresponding particle sizes by PFC3D. We imported the STL-formatted three-dimensional aggregate template created in the earlier step. Then, the small balls were randomly selected within the boundary range of the heterogeneous model, and the small balls were replaced with three-dimensional aggregate with the same shape center and volume as the balls. The operation was repeated until all the small balls were completely replaced. An example of aggregate positions in the three-dimensional heterogeneous model is shown in Figure 4.

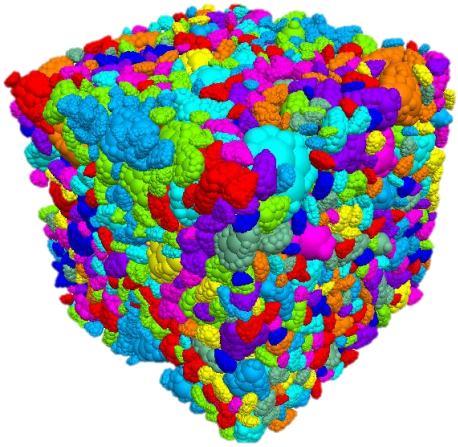

Figure 4. Example of aggregate positions in the three-dimensional heterogeneous model.

(7) The aggregate generation process yields the spatial coordinate information for all aggregates. Small volume units with single material attributes were used to partition the three-dimensional heterogeneous asphalt concrete model. The TXT files were then used to export the spatial coordinate information and the components of small volume units in the asphalt concrete. An example of a small volume unit with single material properties is shown in Figure 5. Then the thermal conductivity was calculated by MATLAB.

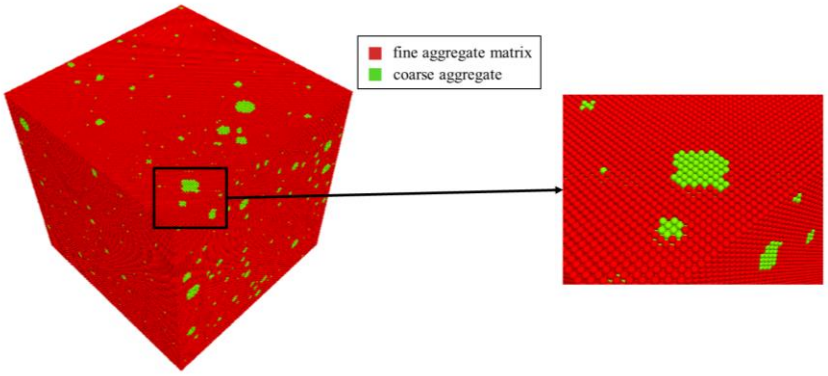

Figure 5. Example of small volume units with single material properties.

3.2. Calculating Thermal Conductivity

According to the homogenization approach proposed by Karim and Krabbenhof [28], the effective thermal conductivity was calculated under this study. First, given a cube region consisting of $2^n \times 2^n \times 2^n$ cells, each small cube cell has a corresponding thermal conductivity determined in the previous section. Figure 6 illustrates the technique for determining the effective thermal conductivity among a representative $2 \times 2 \times 2$ cubes, and the effective thermal conductivity was calculated layer by layer by using space-scale upscaling.

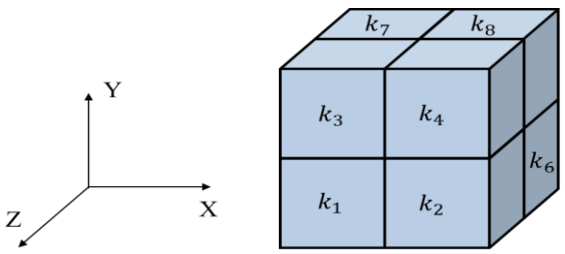

Figure 6. Example of $2 \times 2 \times 2$ cubes.

Therefore, the most basic issue for this method is to devise a method for calculating the effective thermal conductivity for the 2 × 2 × 2 cube units. The effective thermal conductivity of the 2 × 2 × 2 cube units can be expressed as Equation (2) [28]:

$$k_{e,x} = \frac{1}{2}\left[\frac{\frac{k_1k_2}{k_1+k_2} + \frac{k_3k_4}{k_3+k_4} + \frac{k_5k_6}{k_5+k_6} + \frac{k_7k_8}{k_7+k_8}}{(k_1+k_3+k_5+k_7)^{-1} + (k_2+k_4+k_6+k_8)^{-1}}\right]^{\frac{1}{2}} \quad (2)$$

Using the three-dimensional meso-structure model of asphalt concrete described in the preceding section, 128 × 128 × 128 cube units of heterogeneous asphalt concrete were generated based on the aggregate gradation in Table 1. The material composition and effective thermal conductivity of each small cube unit were confirmed by the model, and Equation (2) was used to calculate the effective thermal conductivity of the three-dimensional heterogeneous asphalt concrete model.

Table 1. Aggregate gradation.

Sieve Size (mm)	Passing Percentage (%)	
	Asphalt Concrete	FAM
16	100	100
13.2	96.0	100
9.5	82.1	100
4.75	52.2	100
2.36	30.9	100
1.18	23.0	74.4
0.6	16.9	54.7
0.3	11.0	35.6
0.15	8.4	27.2
0.075	6.8	22.0

4. Model Validation

First, the effective thermal conductivity of the aggregate, FAM, and asphalt concrete were measured experimentally. As mentioned in the previous section, asphalt concrete is regarded as a composite material. Asphalt concrete with an asphalt content of 4.76% and a porosity of 6% was prepared in the laboratory. In this study, the asphalt concrete and FAM have different aggregate gradations and these are listed in Table 1.

When determining the thermal conductivity of solids, the transient plane source technique could be utilized [25]. The transient plane source approach was used to assess the thermal characteristics in order to confirm the validity of model.

When testing asphalt concrete and FAM for their effective thermal conductivity, six cylindrical samples were created in the laboratory with diameters of 100 mm and 50 mm in height. We clamped the sensor with two identical samples, and used a thermal conductivity tester to measure the sample under test, as shown in Figure 7. After the measurement was completed, the sample was removed and the sensor was left to cool down naturally for 20 min. After that, the sample was rotated 180°, and measured again. Asphalt concrete, FAM, and the aggregate were measured 6 times, respectively, and the average of the 6 measurements was thought to be the value of the thermal conductivity of every material. According to the results of the experiment, the average effective thermal conductivity of asphalt concrete, FAM, and the aggregate were 2.127 $Wm^{-1}K^{-1}$, 1.423 $Wm^{-1}K^{-1}$, and 2.855 $Wm^{-1}K^{-1}$, respectively.

Figure 7. Experimental setup.

By using the gradation in Table 1, five random three-dimensional meso-structure models of asphalt concrete were formed. These models were marked as A1~A5, respectively. The effective thermal conductivity of three-dimensional meso-structure models were calculated through Equation (2). Thermal conductivity is seen in Figure 8 as 2.1744 $Wm^{-1}K^{-1}$ on average. The average discrepancy between the experimental and numerical results was 2.34 percent. This shows that the model and calculation method of thermal conductivity used in this paper are reliable.

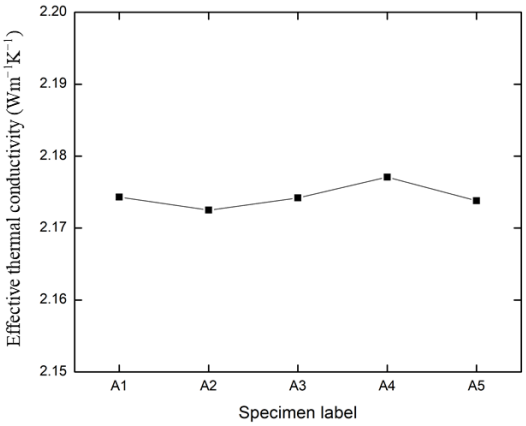

Figure 8. Effective thermal conductivity of three-dimensional meso-structure models of asphalt concrete.

5. Sensitivity Analysis of Thermal Conductivity

5.1. Effects of Coarse Aggregate Orientation Angle and Aspect Ratio

The degree of anisotropy in asphalt concrete is highly correlated with the angle and aspect ratio of the coarse aggregate utilized in that material. To ascertain the impact of aggregate orientation and aspect ratio, three different aggregate orientation angles and five different aggregate aspect ratios were considered, as shown in Table 2. Except for the coarse aggregate in Table 2 having a different orientation and aspect ratio, the other parameters of the asphalt concrete models were the same as those used in the model validation section. The above virtual models were denoted as B1~B15, respectively. The angle between the Z-Axis and X-Axis was known as orientation angle.

Table 2. The aggregate orientation and aspect ratio of asphalt concrete models.

Specimen Label	Orientation Angle of Aggregate (°)	Aspect Ratio of Aggregate
B1	uniformly distributed between 0~30	1
B2	uniformly distributed between 0~30	1.5
B3	uniformly distributed between 0~30	2
B4	uniformly distributed between 0~30	2.5
B5	uniformly distributed between 0~30	3
B6	uniformly distributed between 30~60	1
B7	uniformly distributed between 30~60	1.5
B8	uniformly distributed between 30~60	2
B9	uniformly distributed between 30~60	2.5
B10	uniformly distributed between 30~60	3
B11	uniformly distributed between 60~90	1
B12	uniformly distributed between 60~90	1.5
B13	uniformly distributed between 60~90	2
B14	uniformly distributed between 60~90	2.5
B15	uniformly distributed between 60~90	3

The random generation algorithm of three-dimensional aggregate in this paper was used to obtain the three-dimensional aggregate with different orientation and aspect ratios by changing the parameter setting of the three-dimensional aggregate. Moreover, the effective thermal conductivity of various models with different aggregate orientation and aspect ratios was calculated through the combined prediction method developed in this paper. The result is shown in Figure 9.

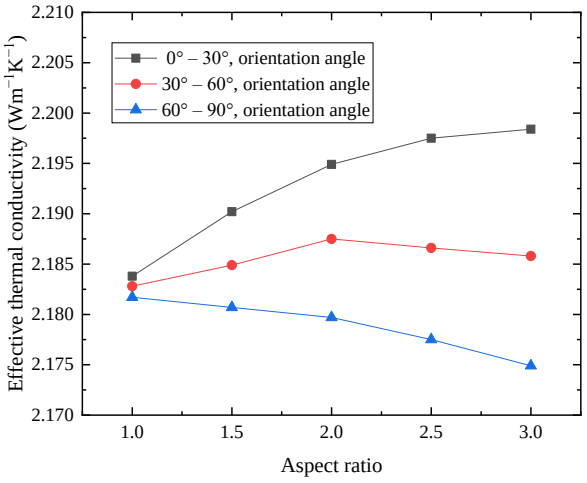

Figure 9. Effects of aggregate orientation angle and aspect ratio on effective thermal conductivity.

Figure 9 indicates that the combined influence of the aggregate orientation angle and aspect ratio, which was consistent with existing literature [26]. All things being equal, it was predicted that with a decreased orientation angle, effective thermal conductivity would increase. For a bigger aspect ratio, this trend is more pronounced. As long as the aspect ratio is one, the effective conductivity of the asphalt concrete was not significantly influenced by the orientation angle. While the aggregate orientation angles were between 0° and 30°, the effective thermal conductivity of asphalt concrete rises as the aggregate aspect ratio increases. Contrarily, the effective thermal conductivity of the asphalt concrete specimens diminishes with increasing coarse aggregate aspect ratio when the aggregate orientation angles are between 60° and 90°. When the orientation of aggregate was between 30~60°, the aspect ratio has small influence on the effective thermal conductivity. As a result, the aggregate has a higher effective thermal conductivity than the asphalt binder does. The effective thermal conductivity of asphalt concrete parallel to the aggregate orientation is

higher when the aggregate orientation is inclined. In the asphalt pavement, the aggregate orientation is closer to the horizontal direction. Thus, it is inferred that utilizing smaller particles reduces the effective thermal conductivity.

5.2. Effects of Coarse Aggregate Content

Obviously, coarse aggregate and FAM in asphalt concrete have a great difference in thermal conductivity. Therefore, when the content of coarse aggregate in asphalt concrete changes, it will alter the contact between the coarse aggregate and the coarse aggregate in asphalt concrete, thus altering the thermal conductivity. The virtual modeling method can control the change of experimental parameters more accurately. In this section, by changing the gradation of virtual specimens, the effects of coarse aggregate content were researched.

Using the gradation in Table 1, four groups of asphalt concrete models were generated in this section, and were marked as C1~C4, respectively. In these four groups of asphalt concrete models, the proportion of aggregate, asphalt, and air voids remained consistent. The ratio of the coarse aggregate to fine aggregate of model C1 is consistent with Table 1 (as the same as A1). In sample C2, the content of coarse aggregates was decreased in the order of the particle size gradation from large to small. Compared with A1, the content of coarse aggregates was decreased by 10% in total. The reduced coarse aggregate was converted into equal volumes of 2.36 mm fine aggregate and was added to the fine aggregate of the sample C2. In the sample C3, the content of the coarse aggregates was decreased in the order of the particle size gradation from large to small. Compared with A1, the content of the coarse aggregates was decreased by 20% in total. The reduced coarse aggregate was converted into equal volumes of 2.36 mm fine aggregate and was added to the fine aggregate of the sample C3. In the sample C4, the content of the coarse aggregates was decreased in the order of the particle size gradation from large to small. Compared with A1, the content of the coarse aggregates was decreased by 30% in total. The reduced coarse aggregate was converted into equal volumes of 2.36 mm fine aggregate and added to the fine aggregate of the sample C4. The effective thermal conductivities of specimens C1~C4 were calculated using the method in this paper. The result are shown in Figure 10.

As shown in Figure 10, replacing coarse particles with 2.36 mm fine aggregates reduces the thermal conductivity, which was similar to previous literature [26]. This illustrates that increasing the content of coarse aggregate can improve the contact between the aggregate in asphalt concrete and increase the thermal conductivity. However, Figure 10 demonstrates that substituting fine aggregate for coarse aggregate had a negligible impact on effective thermal conductivity.

5.3. Effects of Coarse Aggregate with Different Thermal Conductivity

The thermal conductivity of coarse aggregates varies by kind. In order to analyze the effect of various coarse aggregate types on the effective thermal conductivity of asphalt concrete, the combined prediction method was used to calculate. Some typical aggregates were considered in this section. Eight groups of asphalt concrete three-dimensional meso-structure models were generated, and the effective thermal conductivity was calculated, as demonstrated in Figure 11.

Asphalt concrete and coarse aggregate have a nearly linearly positive correlation in terms of effective thermal conductivity. Higher effective thermal conductivity can be achieved by mixing asphalt concrete with marble or granite aggregates. However, the addition of limestone can decrease the effective thermal conductivity. Generally, aggregate thermal properties had a significant impact on the thermal properties of asphalt concrete, which was in accordance with existing literature [14,25].

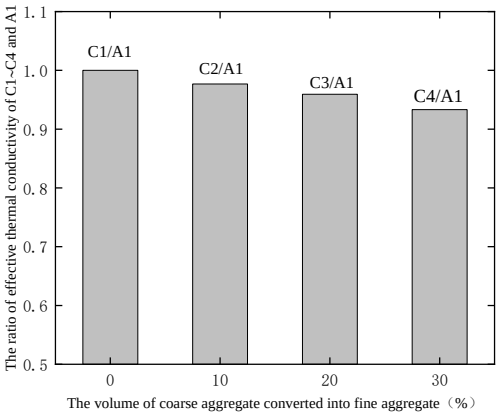

Figure 10. The effective thermal conductivity ratio of C1~C4 to A1.

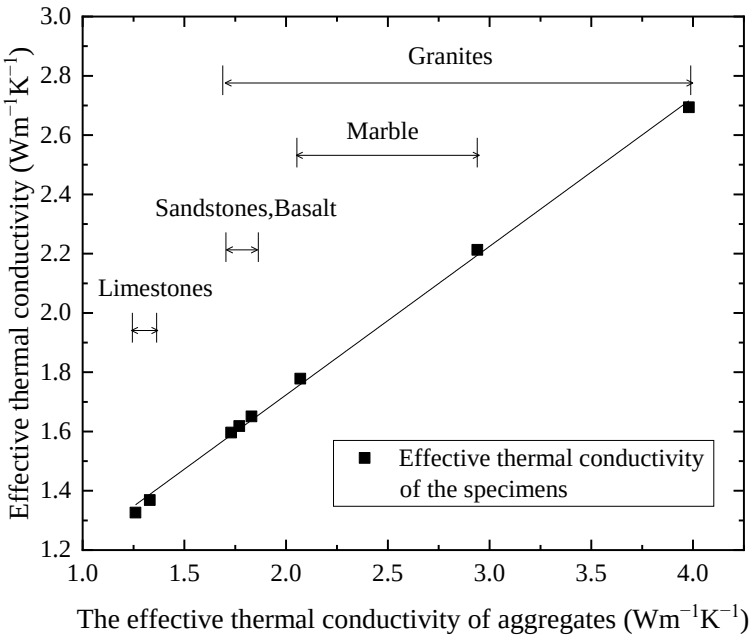

Figure 11. Effect of coarse aggregate type on asphalt concrete thermal conductivity.

5.4. Effects of Air Void

In this article, the asphalt concrete was thought to be a biphasic heterogeneous material. However, when the asphalt mixture is not fully mixed, asphalt concrete may have air voids distributed nonuniformity. Due to the fact that air voids have an influence on the thermal conductivity of asphalt concrete, it is necessary to study this issue further.

In total, 6 sets of three-dimensional heterogeneous asphalt concrete digital specimens were developed, and were marked as D1~D6. The dimensions and material parameters of these digital specimens were the same as those in Section 4. The thermal conductivity of air was set as 0.025 Wm^{-1}K^{-1}. In these 6 groups of specimens, it is assumed that the air voids size was all 1 mm, and six different percentages of the air void were increased from 0% to 10% by 2%, respectively. The effective thermal conductivities of specimens D1~D6 with different air void contents were calculated through the method in this paper, as shown in Figure 12. In general, the prediction results indicated that the thermal conductivity gradually decreased as the air void content increased, which was the same as the results in previous study [25]. Furthermore, each 2% increase in air void reduced the effective thermal conductivity by approximately 3.5%.

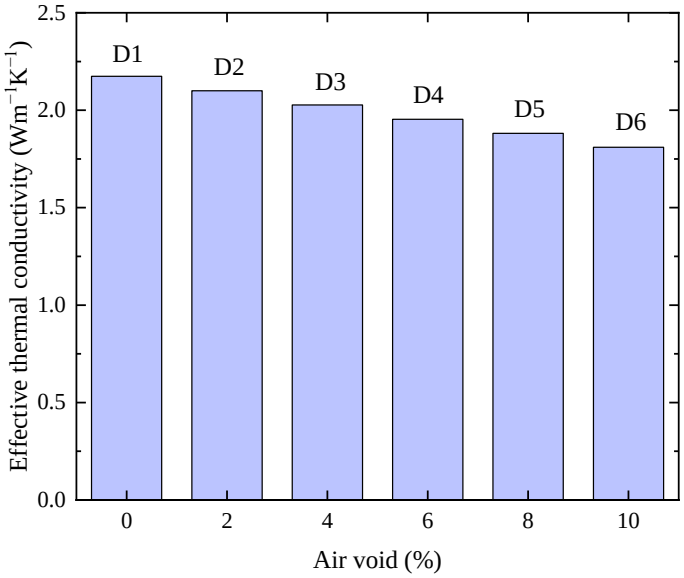

Figure 12. Effect of air void.

To study the distribution nonuniformity of air voids, three groups of cube asphalt concrete specimens were generated, which were noted as E1~E3, respectively. The air voids in specimen E1 were uniformly distributed, and the air voids in specimen E2 and E3 were evenly distributed across the 15% of the total volume of the specimens, as shown in the gray shaded part in Figure 13. All other variables, except the spatial distribution of air voids, were consistent with the stochastic model D4.

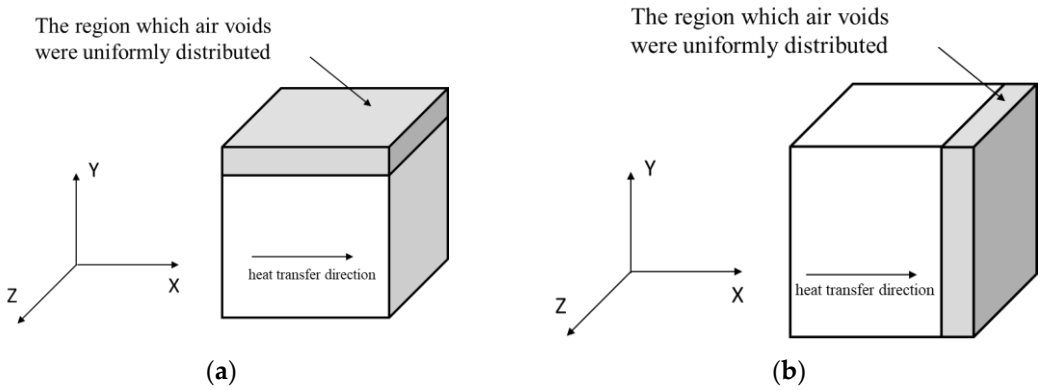

Figure 13. Schematic diagram of air voids distribution in specimen (**a**) E2 and (**b**) E3.

Figure 14 illustrates the predicted effective thermal conductivity from each model. This study found that the air void distribution of asphalt concrete affects its thermal conductivity. Compared with the uniform model (E1), when the pores perpendicular to the thermal conductivity calculation direction (E2) are nonuniform, the effective thermal conductivity will increase, and when the pores parallel to the thermal conductivity calculation direction (E3) are nonuniform, the effective thermal conductivity will decrease.

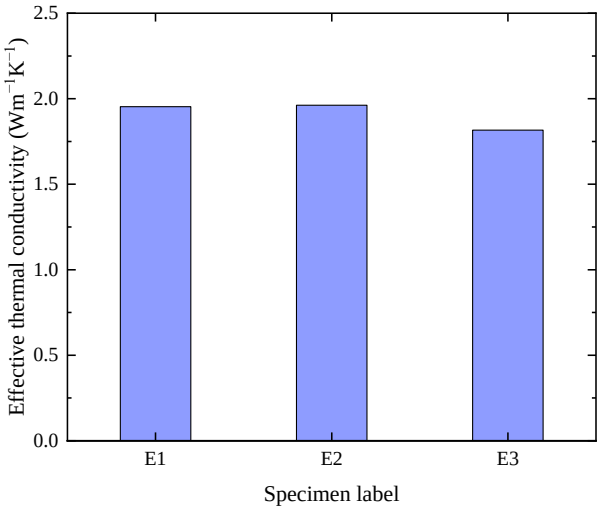

Figure 14. Effect of air void distribution on asphalt concrete thermal conductivity.

When viewing specimen E2 from a macroscopic perspective, it can be regarded as an approximate parallel model, as shown in Figure 13. On the contrary, specimen E3 can be regarded as an approximate series model. Thus, the effective thermal conductivity of specimen E2 could become closer to the theoretical maximum, while that of specimen E3 would be closer to the theoretical minimum. To summarize, the influence of air void nonuniformity on the thermal conductivity mainly depends on the concentration patten of the air voids.

5.5. Effects of Steel Fiber

In some studies [30–32], steel fibers with high thermal conductivity were added to asphalt concrete to enhance the thermal conductivity. In this section, the effect of steel fibers on the thermal conductivity of asphalt concrete was evaluated and verified with the existing experimental data [30].

Long straight steel fibers with an average length of 35 mm and equivalent diameter of 1 mm were used in this paper. The steel fibers had a density of 7.8 g/cm^3 and a thermal conductivity of 46.4 Wm^{-1}K^{-1}. The corresponding heterogeneous meso-structure model of steel fiber asphalt concrete was established using four different contents of steel fiber (0%, 0.5%, 1%, and 1.5%) by weight. The thermal conductivity of the steel fiber asphalt concrete three-dimensional model was calculated, and the results are shown in Figure 15.

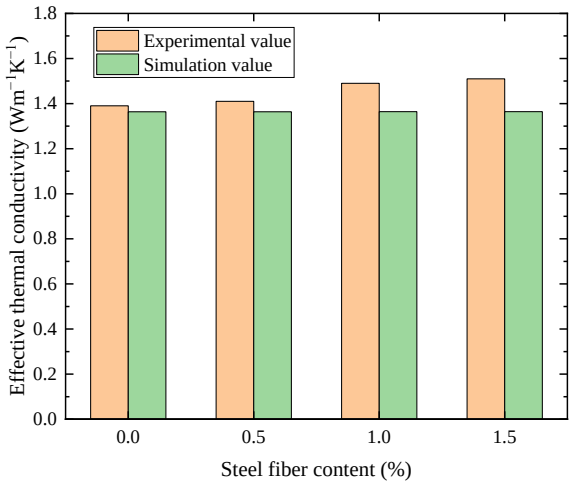

Figure 15. Effect of steel fiber content.

After adding steel fiber with different contents, the difference between the experimental value and the simulated value of effective thermal conductivity of asphalt concrete was 3.2%~9.6%. In general, the effective thermal conductivity increases with the steel fiber percentage.

Three sets of cube asphalt concrete models with varied steel fiber orientations were used to assess the influence of steel fiber orientation on effective thermal conductivity. The above virtual models were denoted as F1~F3, respectively. The steel fibers in F1 were randomly distributed in the asphalt concrete model. The steel fibers in F2 and F3 were parallel to and perpendicular to the direction of thermal flux, respectively. Four different steel fiber contents (0%, 0.5%, 1%, and 1.5%) were considered for each group specimen to calculate the corresponding effective thermal conductivity. As illustrated in Figure 16, the changes in effective thermal conductivity of asphalt concrete caused by different steel fiber orientations were very minor, and the variable ranges of thermal conductivity were less than 0.01 percent. This shows that the steel fiber orientation has a small effect on the effective thermal conductivity, which is negligible. The main reason may be that the steel fiber content needed in the steel fiber asphalt concrete is small, so the orientation has little influence on the effective thermal conductivity.

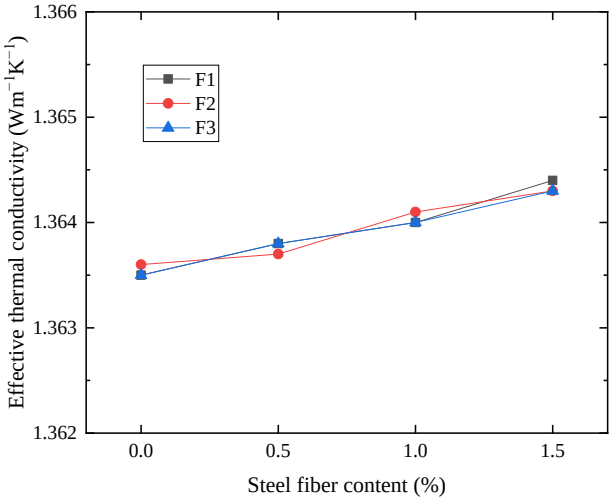

Figure 16. Effect of the steel fiber orientation.

6. Conclusions

This paper developed a combined prediction method for the thermal conductivity of asphalt concrete based on meso-structure and renormalization technology. The analysis concluded as follows:

(1) The relative differences of effective thermal conductivity between the measured and predicted values was 2.34%, which proved the accuracy of the method in this paper.

(2) The effective thermal conductivity was affected by the combination of the aggregate orientation angle and aspect ratio. The effective heat conductivity of asphalt concrete parallel to a specific aggregate orientation tends to be larger when the aggregate orientation tends to be inclined in that direction.

(3) Increasing the coarse aggregate content in asphalt concrete can improve aggregate contact and raise the effective thermal conductivity.

(4) In terms of effective thermal conductivity, asphalt concrete and coarse aggregate have a nearly linearly positive correlation. By combining asphalt concrete with marble or granite aggregates, a higher effective thermal conductivity can be achieved. However, the use of limestone can lower the effective thermal conductivity.

(5) The effective thermal conductivity of asphalt concrete increases as the steel fiber percentage increases. The steel fiber orientation has a small effect on the effective thermal conductivity, which is negligible.

Author Contributions: Conceptualization, J.C.; Formal analysis, X.C.; Writing—original draft, L.Z.; Writing—review & editing, H.D. All authors have read and agreed to the published version of the manuscript.

Funding: This research was funded by the National Natural Science Foundation of China (Grant No. 51908558), Natural Science Foun-dation of Hunan Province (Grant No. 2020JJ5717), Hunan Transportation Science and Technology Project (Grant No. 202017).

Acknowledgments: The authors acknowledge the partial support provided by the National Natural Science Foundation of China (Grant No. 51908558), Natural Science Foundation of Hunan Province (Grant No. 2020JJ5717), Hunan Transportation Science and Technology Project (Grant No. 202017).

Conflicts of Interest: The authors declare no conflict of interest.

References

1. Acharya, T.; Riehl, B.; Fuchs, A. Effects of Albedo and Thermal Inertia on Pavement Surface Temperatures with Convective Boundary Conditions—A CFD Study. *Processes* **2021**, *9*, 2078. [CrossRef]
2. Nwakaire, C.M.; Onn, C.C.; Yap, S.P.; Yuen, C.W.; Onodagu, P.D. Urban Heat Island Studies with emphasis on urban pavements: A review. *Sustain. Cities Soc.* **2020**, *63*, 102476. [CrossRef]
3. Gong, X.; Liu, W.; Ying, H. Phase Change Heat-induced Structure of Asphalt Pavement for Reducing the Pavement Temperature. *Iran. J. Sci. Technol. Trans. Civ. Eng.* **2021**, 1–14. [CrossRef]
4. Chen, J.; Chu, R.; Wang, H.; Zhang, L.; Du, Y. Alleviating urban heat island effect using high-conductivity permeable concrete pavement. *J. Clean. Prod.* **2019**, *237*, 117722. [CrossRef]
5. Aletba, S.R.O.; Hassan, N.A.; Jaya, R.P.; Aminudin, E.; Mahmud, M.Z.H.; Mohamed, A.; Hussein, A.A. Thermal performance of cooling strategies for asphalt pavement: A state-of-the-art review. *J. Traffic Transp. Eng.* **2021**, *8*, 356–373. [CrossRef]
6. Liu, K.; Xu, P.; Wang, F.; You, L.; Zhang, X.; Fu, C. Assessment of automatic induction self-healing treatment applied to steel deck asphalt pavement. *Autom. Constr.* **2022**, *133*, 104011. [CrossRef]
7. Jiao, W.; Sha, A.; Liu, Z.; Li, W.; Jiang, W.; Qin, W.; Hu, Y. Study on thermal properties of steel slag asphalt concrete for snow-melting pavement. *J. Clean. Prod.* **2020**, *277*, 123574. [CrossRef]
8. Zhang, Z.; Luo, Y.; Huang, S.; Zhang, K. Evaluation of temperature reduction and pavement performance of floating beads asphalt mixture. *Int. J. Pavement Eng.* **2019**, *20*, 349–356. [CrossRef]
9. Yan, X.; Chen, L.; You, Q.; Fu, Q. Experimental analysis of thermal conductivity of semi-rigid base asphalt pavement. *Road Mater. Pavement Des.* **2019**, *20*, 1215–1227. [CrossRef]
10. Pan, P.; Wu, S.; Hu, X.; Wang, P.; Liu, Q. Effect of freezing-thawing and ageing on thermal characteristics and mechanical properties of conductive asphalt concrete. *Constr. Build. Mater.* **2017**, *140*, 239–247. [CrossRef]
11. Vo, H.V.; Park, D.-W.; Seo, W.-J.; Yoo, B.-S. Evaluation of Asphalt Mixture Modified with Graphite and Carbon Fibers for Winter Adaptation: Thermal Conductivity Improvement. *J. Mater. Civ. Eng.* **2017**, *29*, 04016176. [CrossRef]
12. Shi, X.; Rew, Y.; Ivers, E.; Shon, C.S.; Stenger, E.M.; Park, P. Effects of thermally modified asphalt concrete on pavement temperature. *Int. J. Pavement Eng.* **2019**, *20*, 669–681. [CrossRef]
13. Shatarat, N.K.; Katkhuda, H.N.; Hyari, K.H.; Asi, I. Effect of using recycled coarse aggregate and recycled asphalt pavement on the properties of pervious concrete. *Struct. Eng. Mech.* **2018**, *67*, 283–290. [CrossRef]
14. Pan, P.; Wu, S.; Hu, X.; Liu, G.; Li, B. Effect of material composition and environmental condition on thermal characteristics of conductive asphalt concrete. *Materials* **2017**, *10*, 218. [CrossRef] [PubMed]
15. Mieczkowski, P.; Budzinski, B. Influence of the Type of HMA and Free Space Content and the Thermal Conductivity Coefficient λ. *IOP Conf. Ser. Mater. Sci. Eng.* **2019**, *603*, 042014. [CrossRef]
16. Maxwell, J.C.A. *Treatise on Electricity and Magnetism*; Clarendon Press: Oxford, UK, 1873.
17. Landauer, R. The Electrical Resistance of Binary Metallic Mixtures. *J. Appl. Phys.* **1952**, *23*, 779–784. [CrossRef]
18. Tavman, I.H. Effective thermal conductivity of granular porous materials. *Int. Commun. Heat Mass Transf.* **1996**, *23*, 169–176. [CrossRef]
19. Wang, J.; Carson, J.K.; North, M.F.; Cleland, D.J. A new approach to modelling the effective thermal conductivity of heterogeneous materials. *Int. J. Heat Mass Transf.* **2006**, *49*, 3075–3083. [CrossRef]
20. Polamuri, D.; Thamida, S.K. Experimental determination of effective thermal conductivity of granular material by using a cylindrical heat exchanger. *Int. J. Heat Mass Transf.* **2015**, *81*, 767–773. [CrossRef]
21. Dan, H.-C.; Zeng, H.-F.; Zhu, Z.-H.; Bai, G.-W.; Cao, W. Methodology for Interactive Labeling of Patched Asphalt Pavement Images Based on U-Net Convolutional Neural Network. *Sustainability* **2022**, *14*, 861. [CrossRef]
22. Gao, L.; Wang, Z.; Xie, J.; Wang, Z.; Li, H. Study on the sound absorption coefficient model for porous asphalt pavements based on a CT scanning technique. *Constr. Build. Mater.* **2020**, *230*, 117019. [CrossRef]
23. Chen, J.; Wang, H.; Dan, H.; Xie, Y. Random modeling of three-dimensional heterogeneous microstructure of asphalt concrete for mechanical analysis. *J. Eng. Mech.* **2018**, *144*, 04018083. [CrossRef]

24. Zhao, Y.; Jiang, J.; Dai, Y.; Zhou, L.; Ni, F. Thermal Property Evaluation of Porous Asphalt Concrete Based on Heterogeneous Meso-Structure Finite Element Simulation. *Appl. Sci.* **2020**, *10*, 1671. [CrossRef]
25. Mirzanamadi, R.; Johansson, P.; Grammatikos, S.A. Thermal properties of asphalt concrete: A numerical and experimental study. *Constr. Build. Mater.* **2018**, *158*, 774–785. [CrossRef]
26. Ren, Z.; Wang, H.; Zhang, L.; Chen, C. Computational analysis of thermal conductivity of asphalt mixture based on a multiscale mathematical model. *J. Eng. Mech.* **2018**, *144*, 04018064. [CrossRef]
27. Chen, J.; Wang, H.; Xie, P.; Najm, H. Analysis of thermal conductivity of porous concrete using laboratory measurements and microstructure models. *Constr. Build. Mater.* **2019**, *218*, 90–98. [CrossRef]
28. Karim, M.R.; Krabbenhoft, K. New renormalization schemes for conductivity upscaling in heterogeneous media. *Transp. Porous Media* **2010**, *85*, 677–690. [CrossRef]
29. Chen, J.; Zhang, L.; Du, Y.; Wang, H.; Dan, H. Three-dimensional microstructure based model for evaluating the coefficient of thermal expansion and contraction of asphalt concrete. *Constr. Build. Mater.* **2021**, *284*, 122764. [CrossRef]
30. Du, Y.; Wang, J.; Deng, H.; Liu, Y.; Tian, J.; Wu, X. Using steel fibers to accelerate the heat conduction in asphalt mixture and its performance evaluation. *Constr. Build. Mater.* **2021**, *282*, 122637. [CrossRef]
31. Du, Y.; Wang, J.; Chen, J. Cooling asphalt pavement by increasing thermal conductivity of steel fiber asphalt mixture. *Sol. Energy* **2021**, *217*, 308–316. [CrossRef]
32. Liu, Q.; Li, B.; Schlangen, E.; Sun, Y.; Wu, S. Research on the Mechanical, Thermal, Induction Heating and Healing Properties of Steel Slag/Steel Fibers Composite Asphalt Mixture. *Appl. Sci.* **2017**, *7*, 1088. [CrossRef]